

## *Meridional Circulation Streamlined*

Deepayan Banik\* and Kristen Menou\*†‡

\*Department of Physics, University of Toronto, 60 St George Street, Toronto, Ontario, M5S 1A7,  
 Canada

† Physics & Astrophysics Group, Dept. of Physical & Environmental Sciences, University of Toronto  
 Scarborough, 1265 Military Trail, Toronto, Ontario, M1C 1A4, Canada

‡ David A. Dunlap Department of Astronomy & Astrophysics, University of Toronto. 50 St. George  
 Street, Toronto, Ontario, M5S 3H4, Canada

(Received 00 Month 20xx; final version received 00 Month 20xx)

Time-dependent meridional circulation and differential rotation in radiative zones are central open issues in stellar evolution theory. We streamline this challenging problem using the ‘downward control principle’ of atmospheric science, under a geostrophic f-plane approximation. New insights emerge from this simplified approach, using pressure as the vertical coordinate. We recover the known stellar physics result that the steady-state meridional circulation decays on the length scale  $(N/2\Omega \times \sqrt{Pr})H$ , assuming molecular viscosity is the dominant drag mechanism. Prior to steady-state, the meridional circulation and the zonal wind (= differential rotation) spread together via radiative diffusion, under thermal wind balance. The corresponding (4th-order) hyperdiffusion process is reasonably well approximated by regular (2nd-order) diffusion on scales of order a pressure scale-height. We derive an inhomogeneous diffusion (equiv. advection-diffusion) equation for the zonal flow which admits closed-form time-dependent solutions in a finite depth domain, allowing rapid prototyping of the meridional circulation pattern. In the weak drag limit, we find that the time to rotational steady-state can be longer than the Eddington-Sweet time and be instead determined by the longer drag time. Unless strong enough drag operates, the internal rotation of main-sequence stars may thus never reach steady-state. Streamlined meridional circulation solutions provide leading-order internal rotation profiles for studying the role of fluid/MHD instabilities (or waves) in redistributing angular momentum in the radiative zones of stars. Despite clear geometrical limitations and simplifying assumptions, one might expect our thin-layer geostrophic approach to offer qualitatively useful results to understand deep meridional circulation in stars.

**Keywords:** Differential rotation; Radiative zone; Downward Control Principle; Hyperdiffusion; Time-dependent penetration

### 1. Introduction

Meridional circulation (Hanasoge 2022) in stars is important for several reasons, including solar activity cycles and dynamo models (Choudhuri *et al.* 1995, Spruit 2002, Weiss and Thompson 2009, Charbonneau 2020), latitudinal distribution of sunspots (Nandy and Choudhuri 2002), advection of angular momentum (Miesch 2000), *tachocline* dynamics (Spiegel and Zahn 1992, Rempel 2005, Garaud and Brummell 2008, Garaud and Arreguin 2009) and the radial transport of chemical species (Elliott and Gough 1999). Even then, it remains poorly understood and crudely treated in state-of-the-art stellar evolution codes such as a MESA (Paxton *et al.* 2010).

Helioseismology (Christensen-Dalsgaard 2002) shows that the outer convective envelope of the Sun ( $0.7 - 1 R_{\odot}$ ), is rotating differentially (Schou *et al.* 1998), while the radiative zone ( $0.2 - 0.7 R_{\odot}$ ) is in approximate solid body rotation (Brown *et al.* 1989, Goode *et al.* 1991). The differential rotation in the convective zone is attributed to different processes like varying

---

\*Corresponding author. Email: deepayan.banik@mail.utoronto.ca

Reynolds stresses arising from turbulent convection (Rüdiger 2022) or torques induced by solar winds (Modisette 1967, Weber and Davis Jr 1967). Therefore, the radiative zone may be conceived as being torqued by the convection zone from above, leading to the generation of meridional circulation via a mechanism called *gyroscopic pumping* (Hughes *et al.* 2007, Garaud and Arreguin 2009, Garaud and Bodenheimer 2010).

It turns out that there is a closely analogous problem in atmospheric science: the *downward control principle* (Haynes *et al.* 1991) proposed to describe the effect of torques due to waves that are dissipated in the upper atmosphere (stratosphere) of the Earth. As the name suggests, torques on the low-density upper layers can exert control on the otherwise inert and dense deeper layers. The process can be understood as follows: alternating *zonal* flows pumped in the upper layer get deflected by Coriolis forces along the *longitudinal* direction similar to Ekman flows (Liu *et al.* 2021) in the ocean. This results in meridionally periodic regions of mass convergence and divergence at the forced level, thereby generating barotropic pressure gradients on all constant-height surfaces “throughout the depth of the fluid” (Showman *et al.* 2006). The pressure gradient causes a return flow in the unforced deeper layers, completing the meridional circulation loop. This return flow, in turn, is again deflected by Coriolis forces, generating a deep zonal flow in the same direction as the top-forced wind. Thus, meridional circulation and zonal flow (differential rotation) penetrate jointly through the depth of the rotating stratified fluid.

Meridional circulation of Sun-like stars has seen several analytical (Eddington 1925, Sweet 1950, Spiegel and Zahn 1992, Garaud and Brummell 2008) and numerical (Clement 1993, Talon *et al.* 2003, Garaud and Arreguin 2009) treatments under the Boussinesq (Rieutord 2006) or the Anelastic (Garaud 2002) approximations inspired from geophysical fluid dynamics. Despite these efforts, the process of penetration arguably lacks a simple, intuitive explanation in the stellar astrophysics literature. Using the aforementioned analogy from atmospheric sciences, we re-consider the problem of meridional circulation in stars and the related issue of the solar tachocline. We argue that the greater physical intuition gained from the atmospheric science perspective outweighs its geometric/simplifying assumptions, making way for a better qualitative understanding of the process. Additionally, we highlight the importance of time-dependent solutions (Elliott 1997, Wood and Brummell 2012, 2018) and extend its applications to the context of stellar evolution codes.

We adopt the primitive  $f$ -plane meteorological framework of Showman *et al.* (2006), which investigates the depth of penetration of zonal jets and their associated meridional circulation into the molecular envelope of Jupiter. In §2, we discuss the assumptions and derive an expression for the steady-state meridional streamfunction, thereby confirming that it decays on the length scale  $(N/2\Omega \times \sqrt{Pr})H$  (Spiegel and Zahn 1992, Garaud 2002). In §3, we derive a single 1D advection-diffusion equation for the zonal velocity in log-pressure coordinates and explain both steady-state and time-dependent analytical solutions, and compare them with Dedalus2 numerical solutions. Finally, we conclude in §4.

## 2. The meridional streamfunction

Figure 1a shows the internal structure of a solar-type star with an outer convective zone, an inner radiative zone, and the core at the center. The zonal, meridional, and vertical coordinates are  $\phi$ ,  $\theta$ , and  $z$ , respectively.

### 2.1. Assumptions

We use the linearized primitive equations of meteorology in pressure coordinates (Holton 1973) to model the radiative zone. The details are elucidated in Showman *et al.* (2006). Our

assumptions are as follows:

- The flow is zonally symmetric *i.e.* quantities do not vary with the azimuthal angle (or longitude),  $\phi$ .
- f-plane (see figure 1a): We use Cartesian coordinates rather than spherical. The f-plane approximation uses a fixed value of the Coriolis parameter  $f (= 2\Omega \sin \theta)$  set to correspond to mid-latitudes ( $\theta = \theta_0$ ). Here  $\Omega$  is the background rotation rate.
- The horizontal extent  $L_y$ , is close to the entire length from the pole to the equator. This stretches the f-plane approximation beyond the formal limit but captures the proper horizontal scale of interest.
- The pressure scale height  $H$  is assumed to be constant, as would happen in an isothermal radiative zone. It is also stably stratified with a Brunt frequency  $N$ .
- A constant gravitational acceleration  $g$  is adopted; for the sun,  $g$  changes by a factor no more than 2 over most of the radiative zone.
- Hydrostatic balance: this is a common assumption in both stellar astrophysics and geophysical fluid dynamics (GFD). It implies that vertical motion with velocity  $w$  is significantly suppressed compared to horizontal velocities  $u$  and  $v$ , which is a direct consequence of the aspect ratio of the flow  $\lambda$  being  $\ll 1$ . We note that a deep radiative zone formally violates the thin layer approximation built in our formalism.
- Geostrophic balance: The Rossby number  $Ro \sim \Delta\Omega/2\Omega$  of the flow is small. Here,  $\Delta\Omega$  is the deviation of the latitudinal differential rotation from the background  $\Omega$ . Inertial forces are therefore dominated by rotation  $\Omega$ .
- The hydrostatic balance and geostrophic balance combine into the thermal wind balance. This implies that a radial gradient in velocity corresponds to a horizontal gradient in temperature.
- Diffusion of momentum and temperature are approximated by linear relaxations (Showman *et al.* 2006); also see appendix A.
- The feedback of the radiative zone on surrounding convection zones is ignored.

## 2.2. The steady-state streamfunction

The independent variables representing the vertical and the meridional coordinates are pressure  $p$  and distance  $y$ , respectively. Time is denoted by  $t$ . The zonal-mean momentum, thermal wind, mass continuity and thermodynamic energy equations for a stratified hydrostatic atmosphere with momentum forcing are given by, respectively,

$$\frac{\partial u}{\partial t} - fv = \frac{u_F - u}{\tau_F} \quad (1)$$

$$fp \frac{\partial u}{\partial p} = R \frac{\partial T'}{\partial y} \quad (2)$$

$$\frac{\partial v}{\partial y} + \frac{\partial w}{\partial p} = 0 \quad (3)$$

$$\frac{\partial T'}{\partial t} - \frac{N^2 H^2}{Rp} w = \frac{T'_E - T'}{\tau_R} \quad (4)$$

where  $u$ ,  $v$ , and  $w (\equiv \partial p / \partial t)$  are the zonal, meridional, and vertical wind speeds in the rotating frame of reference,  $f (= 2\Omega \sin \theta)$  is the Coriolis frequency parameter,  $\theta$  is the latitude and  $R$  is the ideal gas constant. The momentum forcing relaxes  $u$  towards  $u_F$ , and the thermal forcing relaxes  $T$  towards  $T'_E$ . The corresponding frictional drag ( $\tau_F$ ) and radiative ( $\tau_R$ ) relaxation

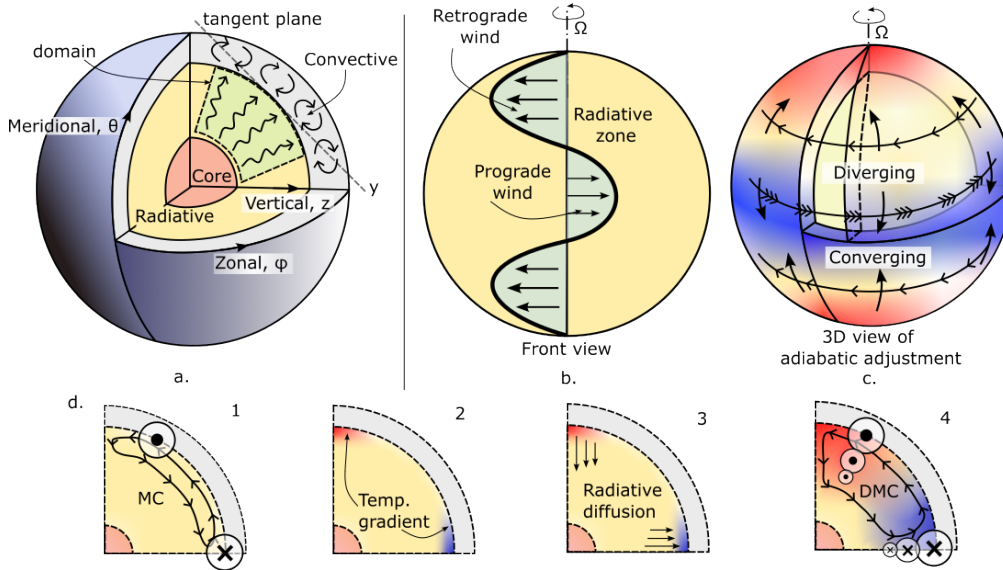


Figure 1. a. The interior structure of a solar-type star showing the convection zone, the radiative zone, the core, the principle coordinates  $(z, y, \phi)$ , and the tangent plane. b. The structure of zonal forcing/torque applied by prograde and retrograde winds at the top of the radiative zone. c. Converging and diverging longitudinal flows due to the action of Coriolis force on the top-forced wind. d. The numbered panels, in order, show the various elements of the meridional circulation. The prograde and retrograde zonal winds are represented by arrows pointing out of and into the plane. The red and blue regions represent the baroclinic structure that results from the zonal torque according to the thermal wind balance. The initial meridional circulation (MC in panel d1) cell is shown as a loop with arrows representing the direction of circulation. The final circulation cell is deep (DMC in panel b4) and corresponds to a smoother vertical gradient of zonal velocity. Note that the schematics do not include any representation for vertical stratification, but it is present in general.

times approximate the usual operators for viscous and heat diffusion. The Brunt frequency  $N$  for the stratified radiative zone with a temperature distribution  $T = T(p) + T'$ , where  $T'$  is a small perturbation from the reference state  $T$ , is given by

$$N = \sqrt{\frac{g}{H} \left( \frac{R}{C_P} - \frac{p}{T} \frac{dT}{dp} \right)}, \quad (5)$$

where  $C_P$  is the specific heat of the constituent gas at constant pressure or along isobars,  $H = RT/g$  is the isothermal scale height, and  $g$  is the acceleration due to gravity. The advection terms in the momentum equation can be ignored in first approximation owing to the low Rossby number  $Ro$  of the flow resulting from geostrophic balance (Showman *et al.* 2006). We thus have four equations (1)-(4) and four variables  $u$ ,  $v$ ,  $w$  and  $T'$ .

In this work, we consider thermal forcing to be zero *i.e.*  $T'_E = 0$  to focus on the role of momentum forcing for meridional circulation. On eliminating  $u$  and  $T'$  from (1)-(4) and substituting  $v$  and  $w$  with their corresponding expressions in terms of the meridional streamfunction  $\psi$  ( $v = -\partial\psi/\partial p$  and  $w = \partial\psi/\partial y$ ), we obtain

$$\frac{p^2}{f\tau_R} \frac{\partial u_F}{\partial p} = \frac{p^2}{\tau_R} \frac{\partial}{\partial p} \left( \tau_F \frac{\partial \psi}{\partial p} \right) + \frac{N^2 H^2}{f^2} \frac{\partial^2 \psi}{\partial y^2}. \quad (6)$$

Our domain of interest is divided into two parts: the top layer corresponds to the near-convection zone where momentum forcing is applied (RHS of equation 1), while the deeper, stably stratified layer below is passive and only driven by the circulation in the top forced layer. The forcing velocity  $u_F$ , relaxation timescales  $\tau_R$  and  $\tau_F$ , and the Rossby deformation radius  $L_D (= NH/f)$  are piecewise constant along the vertical coordinate  $p$ , demarcating the

two layers described. In the passive layer, where  $u_F = 0$ , equation (6) reduces to,

$$L_D^2 \frac{\partial^2 \psi}{\partial y^2} + p^2 \frac{\tau_F}{\tau_R} \frac{\partial^2 \psi}{\partial p^2} = 0 \quad (7)$$

This equation, together with appropriate boundary conditions, gives the steady-state meridional streamfunction in a rotating hydrostatically and geostrophically balanced fluid such as the radiative zone of a Sun-like star. We see that  $\psi$  admits a separable solution of the form  $\psi(p, y) = \psi_p(p)\psi_y(y)$ , with  $\psi_y(y) = \cos(l y)$  *i.e.* periodic in latitude, where  $l (= 1/L_y)$  can represent the latitudinal wavenumber of the shallow jets forced in the top layer. Substituting the above in equation (7) we obtain an ordinary differential equation for the vertical component of the streamfunction  $\psi_p$  as

$$p^2 \frac{\partial^2 \psi_p}{\partial p^2} = \bar{\omega}^2 \psi_p \quad (8)$$

where  $\bar{\omega}^2 = L_D^2 l^2 \tau_R / \tau_F$ . It admits the polynomial solution for  $\psi$ :

$$\psi(p, y) = [A p^{n_1} + B p^{n_2}] \cos(l y) \quad (9)$$

where,  $n_1$  and  $n_2$  are roots of the equation  $n(n-1) = \bar{\omega}^2$ . Constants  $A$  and  $B$  may be determined from interface and boundary conditions. The vertical component of the steady-state streamfunction, which determines the steady-state depth of the meridional circulation, is therefore strictly dependent on  $\bar{\omega}$  which is the product of the Burger number ( $Bu = L_D^2 l^2$ ) and the Prandtl number ( $Pr = \tau_R / \tau_F$ ) as has already been established in literature *e.g.* Spiegel and Zahn (1992), Garaud (2002), Gilman and Miesch (2004), Garaud and Brummell (2008). We now use this setup and formalism to explore the time-dependent behavior of the meridional circulation in a top-forced radiative zone.

### 3. Time-dependent zonal velocity equation

We use the same equations (1)-(4) to derive a single equation for the time-dependent penetration of the zonal wind. In the absence of thermal forcing,  $T'_E = 0$ , and assuming the variables  $u, v, w$  and  $T'$  to be meridionally periodic with a wavenumber  $l$ , so that

$$u = \bar{u} \cos(l y), v = \bar{v} \cos(l y), w = \bar{w} \sin(l y) \text{ and } T' = \bar{T}' \sin(l y), \quad (10)$$

where the barred quantities are functions of  $t$  and  $p$ , we obtain the following from equations (1)-(3) in the passive zone ( $u_F = 0$ ) below the momentum-driven layer,

$$\frac{\partial \bar{u}}{\partial t} - f \bar{v} = \frac{-\bar{u}}{\tau_F} \quad (11)$$

$$f \frac{\partial \bar{u}}{\partial \ln p} = l R \bar{T}' \quad (12)$$

$$l \bar{v} = \frac{\partial \bar{w}}{\partial p} \quad (13)$$

Additionally, assuming a rapid thermal adjustment ( $\partial T' / \partial t = 0$ ) leading to a balance of entropy advection and thermal diffusion, equation (4) gives,

$$\bar{w} = \frac{R \bar{T}' p}{N^2 H^2 \tau_R}. \quad (14)$$

Combining equations (11)-(14) gives us a 1D second-order inhomogeneous diffusion equation for the zonal wind in pressure coordinates:

$$\frac{\partial \bar{u}}{\partial t} + \frac{\bar{u}}{\tau_F} = \frac{\partial}{\partial p} \left( \frac{p^2}{L_D^2 l^2 \tau_R} \frac{\partial \bar{u}}{\partial p} \right) = \left( \frac{\partial k}{\partial z} + k \right) \frac{\partial \bar{u}}{\partial z} + k \frac{\partial^2 \bar{u}}{\partial z^2} \quad (15)$$

where,  $L_D = (NH)/f$  is the Rossby deformation radius, the log-pressure vertical coordinate  $z = \ln p$  and  $k = 1/(L_D^2 l^2 \tau_R)$ . It can be rewritten as a linear advection-diffusion equation for the evolution of the zonal wind (RHS of equation 15). Accounting for the simplification of the radiative diffusion operator as Newtonian linear relaxation, equation (15) shares close similarity with the hyperdiffusion equation obtained for the radial profile of differential rotation by Spiegel and Zahn (1992). In its most general form, equations (15) may have  $L_D, \tau_R, \tau_F$ , and  $k$  that dependent on  $p$ . However, it is possible to find useful approximate analytical solutions to equation (15) if the above parameters are constant. We apply the Dirichlet boundary condition  $\bar{u}(0, t) = u_F$  at the top of the passive domain as an idealized form of zonal forcing. The bottom of the domain has a free slip (no shear) boundary, and hence a Neumann boundary condition given by  $u_z(L, t) = 0$ . Under these conditions, one can use solution C3 in Van Genuchten (1982) for the steady-state,

$$\bar{u}(z) = u_F \left[ \exp\left(\frac{j+k}{2k}z\right) + \frac{j+k}{j-k} \exp\left(-\frac{j-k}{2k}z + \frac{jL}{k}\right) \right] / C(z);$$

$$j = \sqrt{k^2 + \frac{4k}{\tau_F}}; C(z) = 1 + \frac{j+k}{j-k} \exp\left(\frac{jL}{k}\right). \quad (16)$$

An approximate time-dependent solution for the initial condition  $\bar{u}(z, 0) = 0$  can be obtained from C7 in Van Genuchten (1982) and rewritten as

$$\bar{u}(z, t) = \frac{u_F B(z, t)}{2C(z)}; m^\pm = \exp\left(-\frac{k \pm j}{2k}\right); n^\pm = \frac{z \pm jt}{2\sqrt{+kt}};$$

$$B(z, t) = m^- \operatorname{erfc}(n^-) + m^+ \operatorname{erfc}(n^+) + \exp\left(\frac{jL}{k}\right) \times$$

$$\left[ \frac{j+k}{j-k} m^+ \operatorname{erfc}\left(\frac{L}{\sqrt{+kt}} - n^+\right) + \frac{j-k}{j+k} m^- \operatorname{erfc}\left(\frac{L}{\sqrt{+kt}} - n^-\right) \right]$$

$$- \frac{k\tau_F}{2} \exp\left(-L - \frac{t}{\tau_F}\right) \operatorname{erfc}\left(\frac{2L - z - kt}{2\sqrt{+kt}}\right) \quad (17)$$

where ‘erfc’ is the complementary error function. We comment on the limit of validity of this solution in the following section.

#### 4. Applications

Let us consider a radiative zone that is initially under solid body rotation,  $\Omega$ . At time  $t = 0$ , a zonal wind,  $u_F$ , at the outer boundary ( $z = 0$ ) starts torquing this stably stratified layer. A fast, purely dynamical, adiabatic/geostrophic adjustment sets up meridional circulation in a layer, the depth of which depends on the ratio of rotation and stratification  $\Omega/N$ , only. The circulation advects the background stratification to establish a meridional temperature gradient. Section 3 of Spiegel and Zahn (1992) gives a detailed description of the process.

Our solution aims to model the subsequent much slower evolution. The meridional temperature gradient developed in the adjusted layer (see Figure 1d panel 2) also impacts the vertical temperature profiles. Following a rapid thermal adjustment occurring on a short

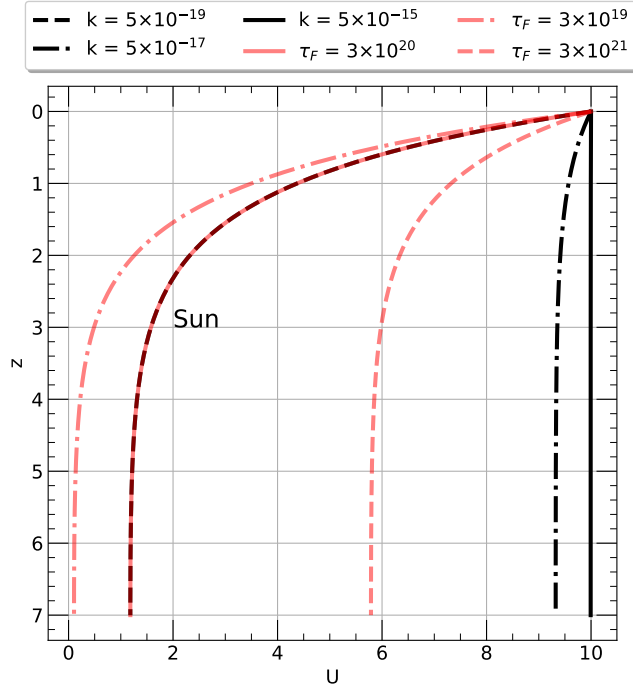


Figure 2. Analytical solution for steady-state zonal wind varying with the vertical coordinate indicating the depth of penetration of the meridional circulation. Different values of  $k$  (black) include the effects of rotation  $f$ , stratification  $N$ , meridional wavenumber  $l$ , scale height  $H$  and the radiative relaxation timescale  $\tau_R$  according to  $k = 1/(L_D^2 l^2 \tau_R)$ . The effect of the viscous drag timescale  $\tau_F$ , on the depth of penetration is shown by red lines. The black dashed line overlapping the red solid line, on the left, depicts the depth of meridional circulation in the radiative zone of the Sun to approximately extend to 2.5 scale heights below the top boundary ( $z = 0$ ), the tachocline.

thermal timescale (Spiegel and Zahn 1992), radiative diffusion propagates the horizontal temperature inhomogeneities further down; Figure 1d panel 3. As a result, the zonal wind and the meridional circulation spread deeper into the radiative envelope (Section 4 Spiegel and Zahn (1992)). The Rayleigh frictional drag (or viscosity) opposes this by acting on the vertical shear of the zonal wind. In steady-state, the meridional circulation penetrates to a depth until these two effects balance each other out. This slower process depends on the Prandtl number in addition to rotation and stratification, as discussed in §2 for the steady-state meridional streamfunction.

#### 4.1. Steady-state zonal velocity

Two main parameters influence the steady-state solution,  $k$  and  $\tau_F$ , as is evident from equation (15). The depth of penetration of zonal velocity and, thus, the meridional circulation crucially depends on both of them. Other parameters that also affect the nature of the solution are the boundary conditions (Garaud and Brummell 2008), namely,  $u_F$  and free shear.

Here,  $k$  accounts for the radiative timescale, rotation, and stratification via  $\tau_R$ ,  $f$ , and  $N$ , respectively. Figure 2 shows vertically varying steady-state zonal wind profiles for different values of  $k$  (black, constant  $\tau_F = 10^{13} \text{ yr s} = 3 \times 10^{20} \text{ s}$ ) and  $\tau_F$  (red, constant  $k = 5 \times 10^{-19} \text{ cm}^2/\text{s}$ ) using expression (16). These are values adopted as representative of the Sun (Menou *et al.* 2004, Menou and Le Mer 2006), the zonal velocity profile for which is labeled in the figure (black dashed, red solid lines). The radiative-convective interface is at  $z = 0$ , and the bottom of the domain is at  $z = \ln(10^3) = 7$ , considering the passive radiative zone to extend through pressures varying three orders in magnitude. The forcing zonal velocity,  $u_F$ , is  $10 \text{ cm/s}$  without loss of generality. The bottom boundary shears freely. Thus, there is no hard constraint on the velocity, allowing it to assume any value.

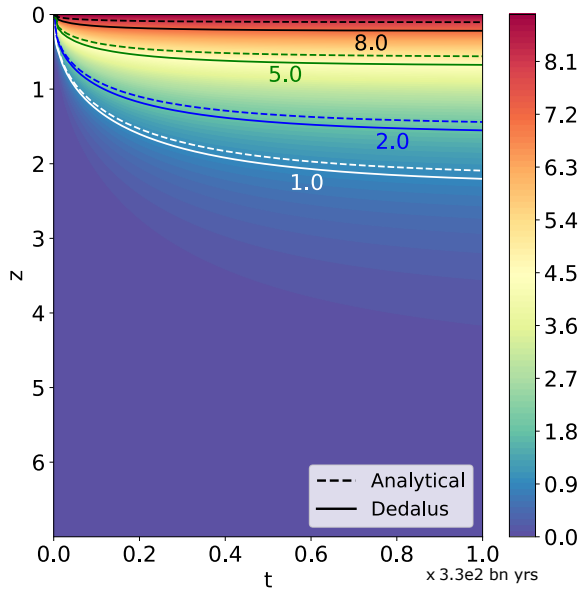


Figure 3. Time-dependent analytical and numerical solutions for the evolution of zonal velocity contours at *early* stages (till  $t = 10^{19}s$ ). The zonal wind forcing  $u_F$  at the radiative-convective interface ( $z = 0$ ) is  $10\text{cm/s}$ . The boundary condition at the bottom is free shear *i.e.*  $\partial u/\partial z = 0$ . The background colormap represents the magnitude of the zonal velocity, as obtained from the analytical solution, at different depths on the ordinate as time proceeds on the abscissa. Specific contours of the numerical Dedalus2 solution is shown using solid lines, while the dashed lines represent the analytical solution in addition to the background colormap. The zonal velocity is seen to decay on a timescale dictated by  $k = 5 \times 10^{-19}$ . This is followed by the slower secondary evolution in figure 4. Note: Maximum value of the zonal velocity at  $z = 0$  is NOT 10. This is a limitation of the analytical solution.

Under strong radiative diffusion *i.e.*, small  $\tau_R$ , the zonal flow, and the corresponding meridional circulation penetrate deep. Greater penetration is also achieved, albeit during adiabatic adjustment, for a weak stratification or strong rotation following the expression of  $k$ . Figure 2 also shows the effect of the frictional drag timescale  $\tau_F$  on the penetration depth. A small  $\tau_F$  corresponds to a stronger drag, limiting the spread from radiative diffusion early so that the zonal velocity forcing cannot penetrate deep, other parameters remaining the same.

From the same figure, the zonal wind is seen to penetrate all the way through the radiative zone of the Sun at *steady state*. This is in reasonable agreement with the *steady-state* estimate made using equation (5.19) of Spiegel and Zahn (1992) by substituting our value of ‘ $\sigma$ ’ (the Prandtl number). Their formulation includes the role of horizontal turbulence rather than frictional drag. However, a value of  $\sigma$  is not specified and is left to general interpretations. Spiegel and Zahn (1992) also have some estimates for the Sun’s *current* degree of penetration in the absence of drag, which will be discussed in the next section.

#### 4.2. Time-dependent penetration

Previous time-dependent studies include Elliott (1997), which numerically solves a set of equations close to Spiegel and Zahn (1992) in spherical coordinates, although reporting results only till one solar age; Wood and Brummell (2012, 2018) perform full-blown three-dimensional numerical simulations of the radiative-convective interface including gravity waves, convective penetration and magnetic fields. They claim that the leading order dynamics are well captured by “balanced” models and may not require complex simulations. This sets the stage for the results obtained from our model, which, as discussed below, provide insights not discussed previously, using a significantly cheaper alternative and succinct explanation.

Figures 3 and 4 compare the time-dependent analytical solutions (cf. expression (17)) with numerical solutions obtained using Dedalus (Burns *et al.* 2020). The temporal evolution of

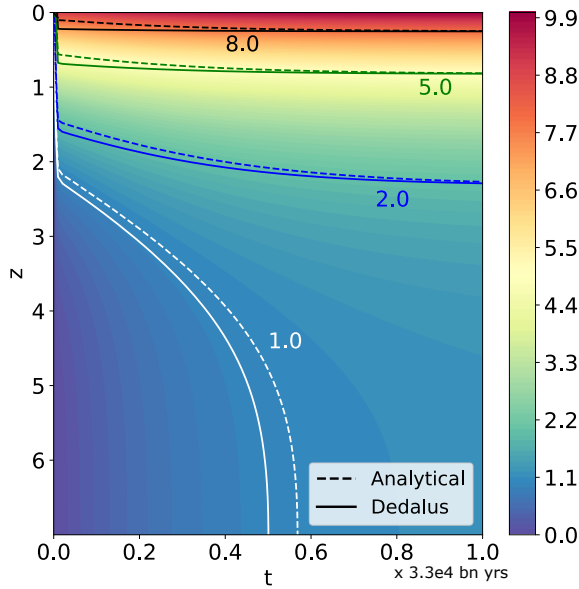


Figure 4. Figure 3 repeated for a longer time extending to  $t = 10^{21} s$  showing both the primary and secondary stages of penetration of the zonal wind. The contour and background colormap description is the same as Figure 3. The fast initial penetration, due to radiative diffusion, is followed by a slower phase over a timescale  $\tau_F = 3 \times 10^{20} s$ . The later occurs when the Rayleigh drag slows the radiative penetration down, finally bringing it to a halt. The zonal velocity penetrates through the entire depth (see contour corresponding to magnitude 1) during this stage owing to a weaker drag. Note: The analytical solution does well at later times.

the zonal velocity is represented as contours on a spacetime plot at *early* and *late* stages, respectively. The value of  $k = 5 \times 10^{-19} \text{ cm}^2/\text{s}$  and  $\tau_F = 10^{13} \text{ yrs} = 3 \times 10^{20} s$ . The dashed and solid lines represent the analytical solution (also the background colormap) and Dedalus, respectively. The different intensities of the zonal wind clearly shows the penetration of the meridional circulation.

Two distinct evolutionary phases are observed: one *fast* and the other *slow*. Neglecting the effect of rotation, stratification, and horizontal and vertical length scales, the aforementioned phases correspond to two competing effects determined by the magnitudes of  $\tau_R$  and  $\tau_F$ . A strong radiative diffusion renders relatively fast penetration. The zonal velocity diffuses to a certain depth in time  $\sim \tau_R$  while obeying the thermal wind balance. The Rayleigh drag, acting weakly, develops gradually and slows the penetration down until it comes to a complete halt on the timescale  $\sim \tau_F$ . At steady-state radiative diffusion and Rayleigh drag balance each other out. This distinctive evolution is clear in the weak drag limit,  $\tau_R < \tau_F$ , as shown in figures 3 and 4. Thus, the time to steady-state is dictated by the longer drag time in this case. The internal rotation profile may therefore never reach steady-state if the drag is too weak, making the time-dependent solution directly relevant. However, in the limit of stronger drag *i.e.*  $\tau_R \gtrsim \tau_F$ , there is simply one evolutionary phase with hardly any penetration.

Figure 5 (right panel) shows the time evolution of zonal velocity in the depths of the Sun, which, under all simplifying assumptions of the current work, must reach *steady-state* in  $3 \times 10^{20} s$  ( $10^{13} \text{ yrs}$ ) or approximately 2000 times its *current* age. Hence, the Sun should run out of hydrogen fuel well before reaching rotational steady-state unless stronger drag is present. The left panel in Figure 5 compares the current and steady-state zonal velocity profiles using our formalism. The steady-state zonal/meridional flow penetrates all the way to the bottom of the radiative zone as also pointed out in Figure 2. In the current Sun, the tachocline extends through 0.75 pressure scale heights to a depth located at  $0.625R_\odot$  from the center of the Sun.

Spiegel and Zahn (1992) present some current-Sun estimates of penetration of differential rotation under various assumptions like zero drag and thin tachocline, amounting to distances

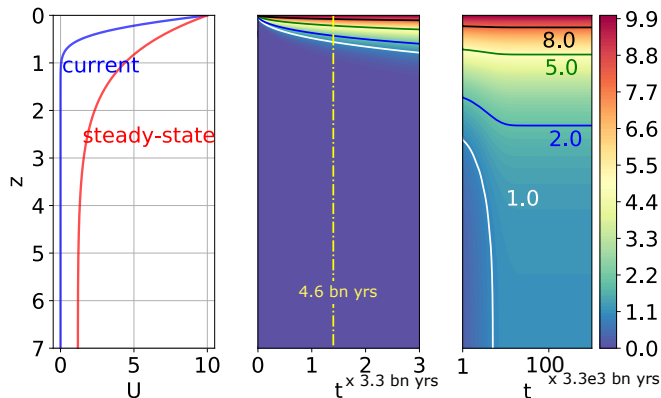


Figure 5. Left panel. Current ( $4.6 \times 10^9$  yrs, solid blue) and steady-state (solid red) zonal velocity profiles varying with depth in the radiative zone of the Sun. The dashed lines show the maximum depth of penetration of the zonal velocity. Right panel. Time evolution of the penetration of zonal wind in the Sun. The dash-dotted yellow vertical line represents the current age of the Sun.

$\sim 0.314R_{\odot}$  and  $0.44R_{\odot}$  from the center of the Sun. These suggest a much deeper penetration than the shallow, helioseismically observed value at  $0.68R_{\odot}$  (Elliott and Gough 1999). In order to truncate the penetration, horizontal turbulence is invoked, which in the strong limit ensures that steady state is reached early enough for theory to match observations. Thus, rotational steady state is not achieved in its main-sequence lifetime lest additional effects such as drag or anisotropic turbulence are invoked.

On the other hand, the parameter  $N/f\sqrt{Pr}$  (say  $\beta$ ) is not a constant for the Sun as shown in Figure 10 of Garaud and Arreguin (2009). Their work suggests that tachocline depth should be restricted to where  $\beta \lesssim 1$  *i.e.*, the region where the Taylor-Proudman regime is not broken. This happens at about  $0.55R_{\odot}$  from the center of the Sun. For comparison, our idealized Sun-model considers a constant value of  $\beta = 0.89$ , which implies a weak Taylor-Proudman constraint, allowing penetration through the entire depth at steady-state.

It is to be noted that the accuracy of the analytical solution is parameter dependent and breaks down at the boundaries because the  $u = 0$  initial condition throughout the domain cannot match the  $u = u_F$  boundary condition. The discrepancy is more apparent at earlier times than late (see maximum colorbar values in both figures 3 and 4). The analytical solution also breaks down when  $k$  and  $1/\tau_F$  differ from one another by more than two orders of magnitude. Also, the linearized Rayleigh drag does not capture the scale dependence of an ordinary 2nd-order differential operator. Similarly, the radiative diffusion should ideally be replaced by a 4th-order hyperdiffusion term as in Spiegel and Zahn (1992). Despite these hefty caveats, the GFD-inspired thin-layer  $f$ -plane solution captures the leading order penetration phenomena with significant accuracy. It can be used to prototype differential rotation profiles in stellar interiors quickly, thereby allowing probes into the onset of magneto/hydrodynamic instabilities(waves) that potentially transport angular momentum in radiative envelopes of main-sequence stars. However, shortcomings of the analytical solution, variable parameters and hyperdiffusion call for detailed numerical solutions.

## 5. Conclusions

We employ the “downward control principle” from atmospheric science to address the time-dependent penetration of meridional circulation and differential rotation in the radiative zones of Sun-like stars due to zonal momentum forcing from the upper convective zone. Assuming geostrophic balance in an  $f$ -plane and adopting pressure as the vertical coordinate, we gain novel insights through a relatively simplified approach.

Our steady-state meridional streamfunction reaffirms the established understanding in stellar physics that the circulation decays over a length scale of  $(N/2\Omega \times \sqrt{Pr})H$ . Rotation and radiative diffusion are drivers of deep penetration, while a stable stratification and viscous drag act to oppose the effect. The differential rotation, which is a combination of the zonal wind and meridional circulation, propagates deep following a fast adiabatic adjustment to the thermal wind balance. We derive a time-dependent, one-dimensional, inhomogeneous diffusion equation which reasonably approximates the fourth-order hyperdiffusion process (Spiegel and Zahn 1992) on a scale comparable to the pressure scale height. Closed-form analytical solutions allow rapid prototyping of differential rotation profiles at any time during the evolution of a main-sequence star.

Spiegel and Zahn (1992) have previously built a steady-state model for the penetration of differential rotation by invoking a strong turbulent (horizontal-only) viscosity to match helioseismic profiles. Using our time-dependent formalism, we also find that a sufficiently strong drag is required to truncate the penetration and reach steady state, otherwise, the internal rotation of main-sequence stars may keep evolving through their lifetime.

Extensions of this work include the study of the effect of mean-molecular weight gradients on the penetration of meridional circulation and the use of computed differential rotation profiles to probe the onset of magneto-/hydrodynamic instabilities in stellar radiative zones, in an attempt to better understand the transport of angular momentum in Sun-like stars.

## Acknowledgements

KM is supported by the National Science and Engineering Research Council of Canada. This work has made extensive use of the following software packages: `numpy`, `matplotlib`, `Dedalus`.

We would furthermore like to acknowledge that this work was performed on land which for thousands of years has been the traditional land of the Huron-Wendat, the Seneca and the Mississaugas of the Credit. Today this meeting place is still the home to many indigenous people from across Turtle Island and we are grateful to have the opportunity to work on this land.

## Data Availability

The data underlying this article is available at: <https://github.com/Textydeep/Meridional-Circulation-Dedalus2.git>.

## References

- Brown, T.M., Christensen-Dalsgaard, J., Dziembowski, W.A., Goode, P., Gough, D.O. and Morrow, C.A., Inferring the Sun's internal angular velocity from observed p-mode frequency splittings. *Astrophysical Journal, Part 1 (ISSN 0004-637X)*, vol. 343, Aug. 1, 1989, p. 526-546., 1989, **343**, 526–546.
- Burns, K.J., Vasil, G.M., Oishi, J.S., LeCoanet, D. and Brown, B.P., Dedalus: A flexible framework for numerical simulations with spectral methods. *Physical Review Research*, 2020, **2**, 023068.
- Charbonneau, P., Dynamo models of the solar cycle. *Living Reviews in Solar Physics*, 2020, **17**, 1–104.
- Choudhuri, A.R., Schussler, M. and Dikpati, M., The solar dynamo with meridional circulation.. *Astronomy & Astrophysics*, 1995, **303**, L29.
- Christensen-Dalsgaard, J., Helioseismology. *Reviews of Modern Physics*, 2002, **74**, 1073.
- Clement, M.J., Hydrodynamical simulations of rotating stars. I-A model for subgrid-scale flow. *The Astrophysical Journal*, 1993, **406**, 651–660.
- Eddington, A., Circulating currents in rotating stars. *The Observatory*, 1925, **48**, 73–75.
- Elliott, J., Aspects of the solar tachocline. *Astronomy and Astrophysics*, 1997, **327**.
- Elliott, J. and Gough, D., Calibration of the thickness of the solar tachocline. *The Astrophysical Journal*, 1999, **516**, 475.

- Garaud, P., On rotationally driven meridional flows in stars. *Monthly Notices of the Royal Astronomical Society*, 2002, **335**, 707–711.
- Garaud, P. and Arreguín, L.A., On the penetration of meridional circulation below the solar convection zone. II. Models with convection zone, the Taylor–Proudman constraint, and applications to other stars. *The Astrophysical Journal*, 2009, **704**, 1.
- Garaud, P. and Brummell, N., On the penetration of meridional circulation below the solar convection zone. *The Astrophysical Journal*, 2008, **674**, 498.
- Garaud, P. and Bodenheimer, P., Gyroscopic pumping of large-scale flows in stellar interiors and application to lithium-dip stars. *The Astrophysical Journal*, 2010, **719**, 313.
- Gilman, P.A. and Miesch, M.S., Limits to penetration of meridional circulation below the solar convection zone. *The Astrophysical Journal*, 2004, **611**, 568.
- Goode, P.R., Dziembowski, W., Korzenik, S. and Rhodes Jr, E., What we know about the Sun’s internal rotation from solar oscillations. *Astrophysical Journal, Part 1 (ISSN 0004-637X)*, vol. 367, Feb. 1, 1991, p. 649–657., 1991, **367**, 649–657.
- Hanasoge, S.M., Surface and interior meridional circulation in the Sun. *Living Reviews in Solar Physics*, 2022, **19**, 3.
- Haynes, P., McIntyre, M., Shepherd, T., Marks, C. and Shine, K.P., On the “downward control” of extratropical diabatic circulations by eddy-induced mean zonal forces. *Journal of the Atmospheric Sciences*, 1991, **48**, 651–678.
- Holton, J.R., An introduction to dynamic meteorology. *American Journal of Physics*, 1973, **41**, 752–754.
- Hughes, D.W., Rosner, R. and Weiss, N.O., *The solar tachocline*, 2007 (Cambridge University Press).
- Liu, W., Liu, Z. and Li, S., The Driving Mechanisms on Southern Ocean Upwelling Change during the Last Deglaciation. *Geosciences*, 2021, **11**, 266.
- Menou, K., Balbus, S.A. and Spruit, H.C., Local axisymmetric diffusive stability of weakly magnetized, differentially rotating, stratified fluids. *The Astrophysical Journal*, 2004, **607**, 564.
- Menou, K. and Le Mer, J., Magnetorotational transport in the early sun. *The Astrophysical Journal*, 2006, **650**, 1208.
- Miesch, M.S., The coupling of solar convection and rotation—(Invited Review). *Solar Physics*, 2000, **192**, 59–89.
- Modisette, J.L., Solar wind induced torque on the sun. *Journal of Geophysical Research*, 1967, **72**, 1521–1526.
- Nandy, D. and Choudhuri, A.R., Explaining the latitudinal distribution of sunspots with deep meridional flow. *Science*, 2002, **296**, 1671–1673.
- Paxton, B., Bildsten, L., Dotter, A., Herwig, F., Lesaffre, P. and Timmes, F., Modules for experiments in stellar astrophysics (MESA). *The Astrophysical Journal Supplement Series*, 2010, **192**, 3.
- Rempel, M., Solar differential rotation and meridional flow: the role of a subadiabatic tachocline for the Taylor–Proudman balance. *The Astrophysical Journal*, 2005, **622**, 1320.
- Rieutord, M., The dynamics of the radiative envelope of rapidly rotating stars-I. A spherical Boussinesq model. *Astronomy & Astrophysics*, 2006, **451**, 1025–1036.
- Rüdiger, G., Differential rotation and stellar convection. In *Differential Rotation and Stellar Convection*, 2022 (De Gruyter: ???).
- Sakurai, T., Spin down problem of rotating stratified fluid in thermally insulated circular cylinders. *Journal of Fluid Mechanics*, 1969, **37**, 689–699.
- Schou, J., Antia, H., Basu, S., Bogart, R., Bush, R., Chitre, S., Christensen-Dalsgaard, J., Di Mauro, M., Dziembowski, W., Eff-Darwich, A. *et al.*, Helioseismic studies of differential rotation in the solar envelope by the solar oscillations investigation using the Michelson Doppler Imager. *The Astrophysical Journal*, 1998, **505**, 390.
- Showman, A.P., Cooper, C.S., Fortney, J.J. and Marley, M.S., Atmospheric Circulation of Hot Jupiters: Three-dimensional Circulation Models of HD 209458b and HD 189733b with Simplified Forcing. *The Astrophysical Journal*, 2008, **682**, 559–576.
- Showman, A.P., Gierasch, P.J. and Lian, Y., Deep zonal winds can result from shallow driving in a giant-planet atmosphere. *Icarus*, 2006, **182**, 513–526.
- Spiegel, E. and Zahn, J.P., The solar tachocline. *Astronomy and Astrophysics*, 1992, **265**, 106–114.
- Spruit, H., Dynamo action by differential rotation in a stably stratified stellar interior. *Astronomy & Astrophysics*, 2002, **381**, 923–932.
- Sweet, P., The importance of rotation in stellar evolution. *Monthly Notices of the Royal Astronomical Society*, 1950, **110**, 548–558.
- Talon, S., Vincent, A., Michaud, G. and Richer, J., A finite volume code for meridional circulation in stars. *Journal of Computational Physics*, 2003, **184**, 244–265.
- Van Genuchten, M.T., *Analytical solutions of the one-dimensional convective-dispersive solute transport equation*, 1982 (US Department of Agriculture, Agricultural Research Service).
- Weber, E.J. and Davis Jr, L., The angular momentum of the solar wind. *Astrophysical Journal*, vol. 148, p. 217–227, 1967, **148**, 217–227.
- Weiss, N. and Thompson, M., The solar dynamo. *Space Science Reviews*, 2009, **144**, 53–66.
- Wood, T.S. and Brummell, N.H., Transport by meridional circulations in solar-type stars. *The Astrophysical Journal*, 2012, **755**, 99.
- Wood, T.S. and Brummell, N.H., A self-consistent model of the solar tachocline. *The Astrophysical Journal*, 2018, **853**, 97.

## Appendix A: Hyperdiffusion

In this appendix, we make a further connection to the hyperdiffusion solutions of Sakurai (1969), Spiegel and Zahn (1992). Replacing the linear relaxation for temperature perturbations by the usual 2nd order heat diffusion operator in equation (4) and separating out the horizontal coordinate  $y$ , leaves us with the following replacement to equation (14),

$$\bar{w} = - \left( \frac{\kappa}{H^2} \right) \left( \frac{Rp}{N^2 H^2} \right) \frac{\partial^2 \bar{T}}{\partial z^2}. \quad (\text{A.1})$$

Here,  $\kappa$  is the coefficient of radiative heat diffusion. Combining equations (11-13) and (A.1) we get

$$\frac{\partial \bar{u}}{\partial t} + \frac{\bar{u}}{\tau_F} = \frac{\partial}{\partial p} \left( \frac{-\kappa p}{L_d^2 l^2 H^2} \frac{\partial^3 \bar{u}}{\partial (\ln p)^3} \right) = -k \frac{\partial^3 \bar{u}}{\partial z^3} - k \frac{\partial^4 \bar{u}}{\partial z^4} \quad (\text{A.2})$$

where  $k = \kappa / (l L_D H)^2$ , is the same as  $k = 1 / (L_D^2 l^2 \tau_R)$  mentioned previously in §3, assuming we set  $\tau_R = H^2 / \kappa$ . By comparing our hyperdiffusion equation to that in Spiegel and Zahn (1992), we recognize a similar 4th-order diffusive operator. However, the inhomogeneous nature of hyperdiffusion in our equation differs from the homogeneous result in Spiegel and Zahn (1992), possibly because of the thin layer assumption ( $h \ll H$ ) adopted in their work.

Dimensional analysis shows that the regular 2nd-order diffusion evolves on a time scale of order  $z^2 \tau_R$ . By contrast, the 4th-order hyperdiffusion operator evolves on a time scale of order  $z^4 \tau_R$ . These two timescales match for  $z = 1$ , i.e., on a scale equal to the pressure scale height  $H$ , which is also the scale we chose to relate  $\tau_R$  and  $\kappa$ . In other words, we expect a regular diffusion treatment to approximate the actual hyperdiffusion process relatively well on scales of order  $H$ . We also note that the rather large scale height  $H \sim 0.1 R_\odot$  in a main sequence star like the Sun implies a modest dynamic range of only  $z \sim 1-7$  over the full radiative zone.

We also recognize that linear relaxation is usually applicable to optically thin media, while the radiative stellar interior is optically thick. We argue that linear relaxation, which is a first-order approximation for the regular diffusion operator, may be used so long the perturbation temperature is significantly smaller than the background profile i.e. the temperature does not vary drastically with height in the medium (Showman *et al.* 2008).

For all these reasons, we focus on a simpler second-order diffusion treatment in our main discussion to gain insight and obtain leading-order results. We recognize that numerical solutions to the exact hyperdiffusion equation A.2 could be obtained relatively easily and would be necessary when the parameters in the hyperdiffusion equation vary with coordinates  $z$ . Nevertheless, we expect the main understanding gained from our second-order diffusion analysis with constant parameters to remain broadly valid and useful.

## Appendix B: Vertically varying radiative diffusion

We use Dedalus2 to solve equation (15) with  $k$  varying in the vertical, which is the more generally relevant scenario. We see the steady-state zonal wind profiles in Figure B1 (right panel) corresponding to different depths at which radiative diffusion is shut off (left panel). That radiative diffusion is the clear driver of deep penetration is evident from the truncation of the spread of zonal wind in the lower region for models with larger Prandtl number. Another feature is the accumulation of kinetic energy in the strongly radiative-diffusive upper region, leading to higher-magnitude winds. The shallower this region of energy accumulation, the stronger the wind.

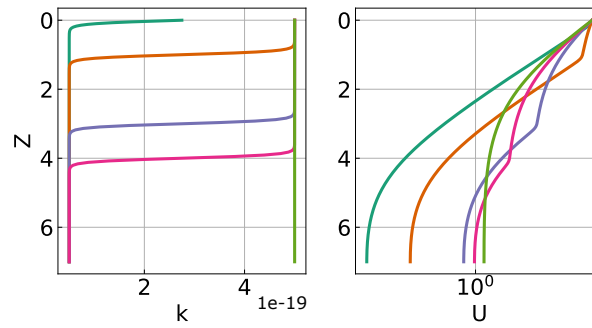


Figure B1. Domain-dependent profiles of  $k$  and the corresponding steady-state zonal velocity profiles that result from them. The maximum value of  $k$  is the same as that for the Sun, and the minimum value is one-tenth the maximum. The x-axis of the second plot is in log-scale and clearly shows the accumulation of kinetic energy in the radiatively diffuse upper layer. See text for details.